



Article

# Determination of IgG1 and IgG3 SARS-CoV-2 Spike Protein and Nucleocapsid Binding—Who Is Binding Who and Why?

Jason K. Iles <sup>1,2</sup>, Raminta Zmuidinaite <sup>1,2</sup>, Christoph Sadee <sup>3,4</sup>, Anna Gardiner <sup>1</sup>, Jonathan Lacey <sup>1</sup>, Stephen Harding <sup>5</sup>, Gregg Wallis <sup>5</sup>, Roshani Patel <sup>5</sup>, Debra Roblett <sup>3</sup>, Jonathan Heeney <sup>2,6</sup>, Helen Baxendale <sup>7</sup> and Ray Kruse Iles <sup>1,2,8,\*</sup>

<sup>1</sup> MAPSciences, The iLab, Stannard Way, Bedford MK44 3RZ, UK; jasoniles51@googlemail.com (J.K.I.); Raminta.Zmuidinaite@mapsciences.com (R.Z.); Anna.Gardiner@mapsciences.com (A.G.); Jonathan.Lacey@mapsciences.com (J.L.)

<sup>2</sup> Laboratory of Viral Zoonotics, Department of Veterinary Medicine, University of Cambridge, Madingley Road, Cambridge CB3 0ES, UK; jlh66@cam.ac.uk

<sup>3</sup> The Francis Crick Institute, 1 Midland Road, London NW1 1AT, UK; ch.y.sadee@gmail.com (C.S.); debbie.roblett@crick.ac.uk (D.R.)

<sup>4</sup> Department of Neuromuscular Diseases, UCL Queen Square Institute of Neurology, Queen Square, London WC1N 3BG, UK

<sup>5</sup> The Binding Site Group Ltd., 8 Calthorpe Road, Edgbaston, Birmingham B15 1QT, UK; stephen.harding@bindingsite.com (S.H.); Gregg.Wallis@bindingsite.com (G.W.); Roshani.Patel@bindingsite.com (R.P.)

<sup>6</sup> DIOSynVax, University of Cambridge, Madingley Road, Cambridge CB3 0ES, UK

<sup>7</sup> Royal Papworth Hospital NHS Foundation Trust, Cambridge CB3 0ES, UK; hbaxendale@nhs.net

<sup>8</sup> NISAD, Sundstorget 2, 252-21 Helsingborg, Sweden

\* Correspondence: Ray.Iles@mapsciences.com

**Citation:** Iles, J.K.; Zmuidinaite, R.; Sadee, C.; Gardiner, A.; Lacey, J.; Harding, S.; Wallis, G.; Patel, R.; Roblett, D.; Heeney, J.; et al.

Determination of IgG1 and IgG3 SARS-CoV-2 Spike Protein and Nucleocapsid Binding—Who Is Binding Who and Why? *Int. J. Mol. Sci.* **2022**, *23*, 6050. <https://doi.org/10.3390/ijms23116050>

Academic Editor: Irmgard Tegeder

Received: 18 March 2022

Accepted: 25 May 2022

Published: 27 May 2022

**Publisher's Note:** MDPI stays neutral with regard to jurisdictional claims in published maps and institutional affiliations.



**Copyright:** © 2022 by the authors. Licensee MDPI, Basel, Switzerland. This article is an open access article distributed under the terms and conditions of the Creative Commons Attribution (CC BY) license (<https://creativecommons.org/licenses/by/4.0/>).

**Abstract:** The involvement of immunoglobulin (Ig) G3 in the humoral immune response to SARS-CoV-2 infection has been implicated in the pathogenesis of acute respiratory distress syndrome (ARDS) in COVID-19. The exact molecular mechanism is unknown, but it is thought to involve this IgG subtype's differential ability to fix, complement and stimulate cytokine release. We examined the binding of convalescent patient antibodies to immobilized nucleocapsids and spike proteins by matrix-assisted laser desorption/ionization–time of flight (MALDI-ToF) mass spectrometry. IgG3 was a major immunoglobulin found in all samples. Differential analysis of the spectral signatures found for the nucleocapsid versus the spike protein demonstrated that the predominant humoral immune response to the nucleocapsid was IgG3, whilst for the spike protein it was IgG1. However, the spike protein displayed a strong affinity for IgG3 itself, as it would bind from control plasma samples, as well as from those previously infected with SARS-CoV-2, similar to the way protein G binds IgG1. Furthermore, detailed spectral analysis indicated that a mass shift consistent with hyper-glycosylation or glycation was a characteristic of the IgG3 captured by the spike protein.

**Keywords:** COVID-19; convalescent plasma; spike protein; nucleocapsid; IgG1; IgG3; predictive profile

## 1. Introduction

The rapidly developing COVID-19 disease syndrome is a delayed event following initial infection of the upper respiratory tract, followed by lower respiratory tissue involvement and a progressive hyper-inflammatory immune response [1]. Somewhat counterintuitively, the marked feature of those requiring hospital treatment is the extremely high titre of antibody and cytokine elevation in those with severe COVID-19 disease [2,3]. However, despite such a massive immune response, the alveoli cells and the blood stream are invaded by viral particles [4].

The humoral response to SARS-CoV-2 is primarily directed towards the nucleocapsid (N protein) and the spike protein (S protein) complex [5]. By the time of ARDS onset, the initial IgM antibody response to the virus has declined and is replaced by IgA and IgG antibodies. IgG is the most abundant class of antibody found in the convalescent plasma of those recovering from COVID-19 ARDS [6] and the onset of ARDS appears to correspond with the time of the antibody class switch to IgG [7] (see Figure 1A). Antibody responses directed at the spike protein and the receptor binding domain (RBD) in particular, have been identified as the main neutralizing component of the SARS-CoV-2 antibody response [8–10]. A distinct antibody signature has been linked to different COVID-19 disease outcomes; early spike-specific responses were associated with a positive outcome, while early nucleocapsid-specific responses were associated with a negative outcome and death. Furthermore, the fragment crystallizable (Fc)-associated functions of the antibody response such as antibody-mediated phagocytosis, cytotoxicity and complement deposition are critical for disease resolution [11].

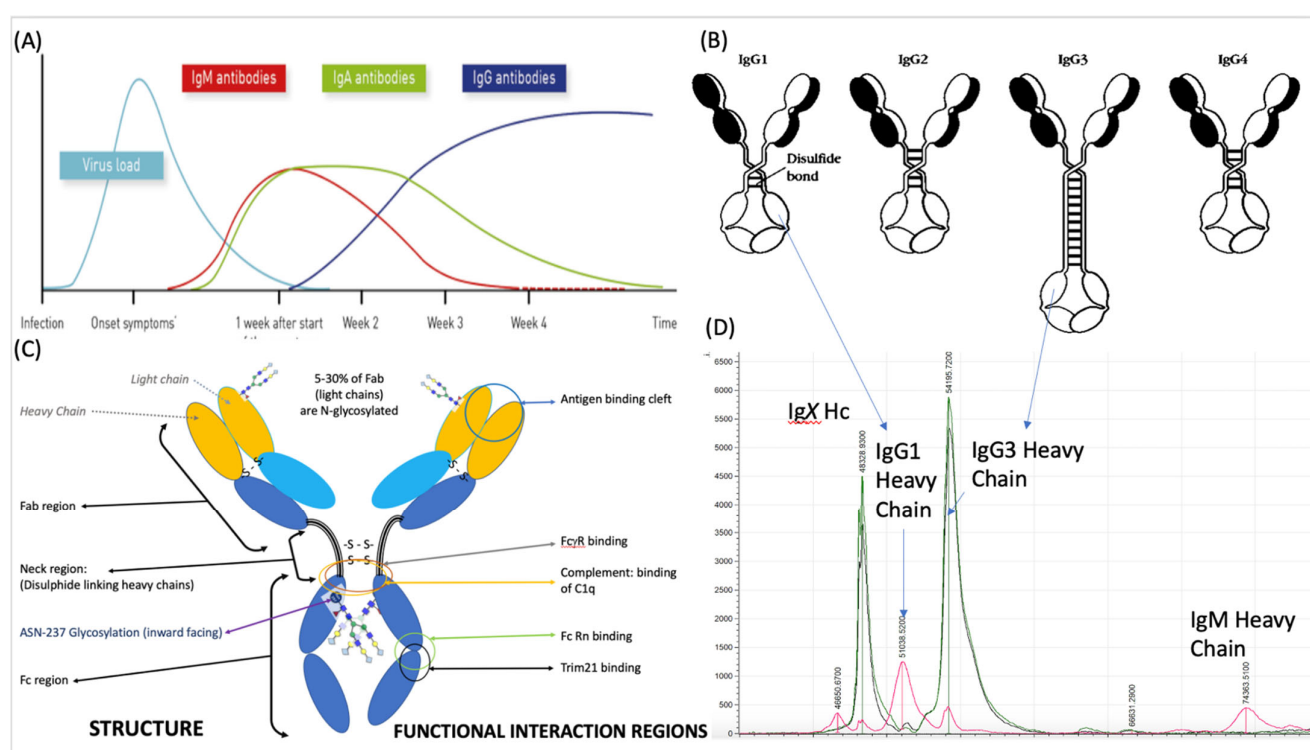


**Figure 1.** A schematic of the humoral response–immunoglobulin major class switching following SARS-CoV-2 infection and COVID-19 progress is illustrated in (A). IgG predominates 3–4 weeks after the onset of symptoms and the major structural and functional domains of IgG are also illustrated. The variation in the neck region of the 4 subclasses of human IgG are shown in (B), while (C) shows structure and functional interaction regions of immunoglobulin. IgG3 is the largest and its heavy chain (Hc) resolution in MALDI-ToF mass spectra (D) is indicated at 54,000  $m/z$  (IgG3 Hc). Also indicated is the IgG1 heavy chain (IgG1 Hc), which resolves at 51,000  $m/z$ . The position of the IgM heavy chain peak (IgM Hc) is indicated at 74,000  $m/z$ . An Ig (IgX Hc), which is thought to be either IgG2 or IgG4 but has yet to be fully identified, was found in patient samples, and is shown at 49,000  $m/z$ .

IgG consists of four sub classes, each with structural differences within and adjacent to the hinge region associated with Fc receptor binding and complement activation (see Figure 1C and Table 1). A highly elevated and disproportionate IgG subclass response, dominated by IgG3, has been implicated as a discriminant marker of adverse outcomes in COVID-19 patients [12].

**Table 1.** Descriptive comparison of physical structure and functional biological differences between the four human IgG subclasses.

	IgG1	IgG2	IgG3	IgG4
Relative Serum abundance	43-75%	16-48%	1.7-7.5%	0.8 - 11.7%
Mean adult serum level (g/L)	6.98 g/L	3.8 g/L	0.51 g/L	0.56 g/L
Half-life (days)	21	21	7 to 21	21
Responses to: Protein	++	+/-	++	++
Polysaccharides	+	+++	+/-	+/-
Allergens	+	(-)	(-)	++
<b>Total mass *</b>	146 kDa	146 kDa	170 kDa	146 kDa
Average observed Kappa			23 kDa	
Average observed Lambda			24 kDa	
Average observed Heavy chain	51 kDa	51 kDa	56 kDa	49 kDa
Heavy chain N-linked Glyc sites	1	1	2	1
Heavy chain O-linked Glyc sites	0	0	3	0
Amino acids in hinge region	15	12	62	12
Inter-chain disulphide	2	4	11	2
C1q binding	++	+	+++	-
Receptors binding:				
Fcγ-RI	+++	-	+++	+
Fcγ-RIIa	++	+/-	++	+/-
Fcγ-RIIb/c	++	+/-	++	++
Fcγ-RIIIa	+	+/-	+++	+/-
Fcγ-RIIIb	+/-	+/-	+	-
FcRn	+++	+++	++/+++	+++
Placental transfer	+++	++	++/+++	+
Protein G binding	++	++	++	+
Protein A binding	++	++	-	++

\* Mass as determined by sodium dodecyl sulphate–polyacrylamide gel electrophoresis (SDS-PAGE).

Binding proteins (antibodies in particular) were captured from convalescent patient plasma samples and examined by MALDI-ToF mass spectrometry. The mass spectral signatures of Ig species, IgG subclasses and, in particular, their respective heavy chains, were matched and quantified (Figure 1D). Here we report the comparison of IgG1 and IgG3 (captured by immobilized N-proteins and spike proteins) in relation to disease severity post SARS-CoV-2 infection.

## 2. Results

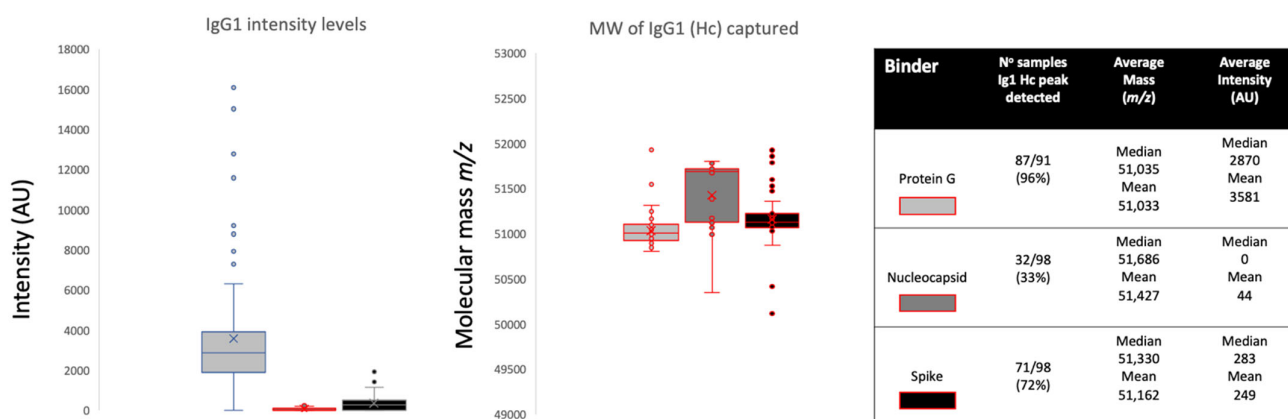
Post elution from respective antigen-coupled magnetic beads, MALDI-ToF mass spectra were obtained and peaks were recorded. These were matched against reference MALDI-ToF mass spectra obtained from the preparation of purified human serum

proteins run under the same reducing and acetic acid pH conditions: human serum albumin (HSA), Transferrin (Merck Life Science UK Ltd., Dorset, UK), IgG1, IgG3, IgA and IgM (Abcam, Discovery Drive, Cambridge, Biomedical Campus, Cambridge, UK).

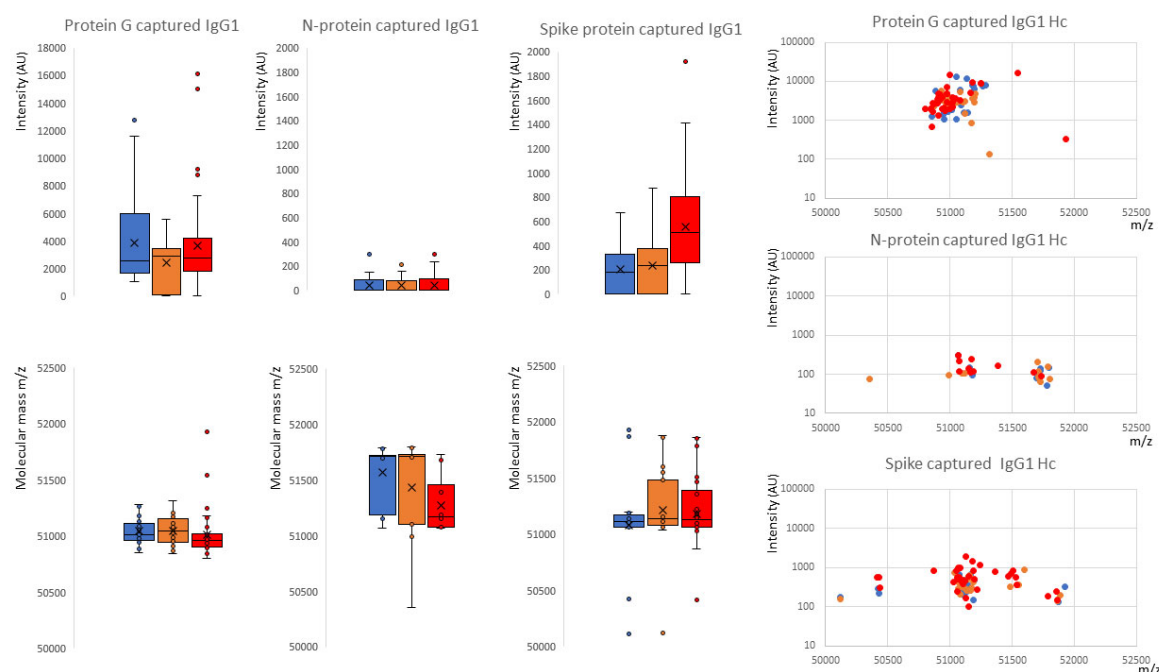
Data from the pooled polyclonal immunoglobulin isolate showed that IgG1 heavy chains averaged at a peak apex  $\sim 51,000$   $m/z$ , IgG3 at  $\sim 54,000$   $m/z$ , IgA at  $\sim 56,000$   $m/z$  and IgM at  $\sim 74,000$   $m/z$ . Human albumin was at  $66,400$   $m/z$  (1+) and Transferrin was at  $\sim 79,600$   $m/z$ . All were broad heterogeneous peaks reflecting glycosylation/glycation and sequence variation. In the protein G, nucleocapsid and spike protein magnetic bead isolates, the dominance of IgG1 was almost always lost, which gave way to IgG3 peak prominence at  $\sim 54,000$   $m/z$  and a peak at  $\sim 49,000$   $m/z$ . The latter has revealed common peptide sequence fragment matches for IgG following formic acid lysis, but a precise identity confirmation as IgG2 or IgG4 has yet to be established (unpublished data) (see Figure 1D). IgA peaks at  $\sim 56,000$   $m/z$  and IgM peaks at  $\sim 74,000$   $m/z$  could be detected in some samples, but they were always smaller (at least 1/20th) than the IgG subclasses' peak intensities. This study focuses on the binding of IgG1 and IgG3 to antigens.

### 2.1. IgG1 Levels and Molecular Mass

Looking at the overall binding from all samples, protein G magnetic beads bound large amounts of IgG1 (peak detected in 96% of samples, median intensity 2870 arbitrary units (AU)), nucleocapsid beads bound very little (peak detected in 33% of samples, median intensity 0AU) and spike protein beads bound a smaller but significant quantity (peak detected in 72% of samples, median intensity 283AU) (see Figure 2). Comparing the three sample groups, protein G bound equally high amounts of IgG1 from sero-negative healthcare workers (HCWs), sero-positive HCWs with mild symptoms and COVID-19 ARDS patient samples (see Figure 3), thus reflecting the polyclonal (non-antigen specific) binding of IgG1 by protein G. Nucleocapsid magnetic beads displayed equally low IgG1 levels in all three sample groups. Hence, there were no significant anti-nucleocapsid IgG1 antibodies, nor binding of polyclonal IgG1 by nucleocapsid proteins. Prefusion complete spike protein displayed the lowest binding of IgG1 in the sero-negative HCW samples (peak detected in 60% of samples, median intensity 186AU), higher levels in the sero-positive HCWs (peak detected in 61% of samples, median intensity 283AU) and significantly higher levels in the COVID-19 ARDS patient samples (peak detected in 92% of samples, median intensity 507AU) (Figure 3 and Figure 4A). Therefore, this finding reflected specific anti-spike IgG1 binding to the immobilized spike protein.

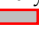
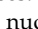



**Figure 2.** Relative intensities and variance in peak apex molecular mass of IgG1 heavy chains (IgG1 Hc) recovered from the same samples by protein G, nucleocapsid and stabilized spike protein. The non-parametric Kruskal–Wallis statistical test was carried out to test differences between study cohorts. The  $p$  values (alpha: 0.05) were as follows: intensity  $p < 0.0001$  and molecular mass  $p < 0.0001$ .



**Figure 3.** Distribution of intensity for captured and eluted IgG1 heavy chains (IgG1 Hc) and the relative peak molecular mass being bound. The dot plots to the right are intensity versus molecular mass for individual samples; Blue represents data from SARS-CoV-2 sero-negative HCWs, orange from SARS-CoV-2 sero-positive HCWs having recovered from mild symptoms and red sample data from convalescent patients recovering from COVID-19 ARDS. The non-parametric Kruskal–Wallis statistical test was carried out to test differences between study cohorts. The  $p$  values (alpha: 0.05) were as follows: protein G capture intensity  $p = 0.66$ , molecular weight  $p = 0.038$ ; protein N capture intensity  $p = 0.84$ , molecular weight  $p = 0.15$ ; protein S capture intensity  $p = 0.0003$ , molecular weight  $p = 0.63$ .

(A) IgG1					(B) IgG3				
Binder	Study group	N° samples Ig1 HC peak detected	Average Mass (m/z)	Average Intensity (AU)	Binder	Study group	N° samples Ig3 HC peak detected	Average Mass (m/z)	Average Intensity (AU)
Protein G (median peak m/z -51,005)	HCW Sero negative	30/30 (100%)	Medium 51,017 Mean 51,043	Median 2574 Mean 3881	Protein G (median peak m/z -54,126)	HCW Sero negative	10/30 (33%)	Medium 54,137 Mean 54,117	Median 0 Mean 933
	HCW Sero positive	24/24 (100%)	Medium 51,045 Mean 51,048	Median 2904 Mean 2414		HCW Sero positive	12/24 (39%)	Medium 54,124 Mean 54,087	Median 0 Mean 368
	Patient- COVID-19 ARD	33/37 (89%)	Medium 50,960 Mean 51,014	Median 2786 Mean 3638		Patient- COVID-19 ARD	0/37 (0%)	Medium ND Mean ND	Median 0 Mean 0
Nucleocapsid (median peak m/z - 51,686)	HCW Sero negative	11/30 (37%)	Medium 51,710 Mean 51,569	Median 0 Mean 46	Nucleocapsid (median peak m/z - 54,267)	HCW Sero negative	12/30 (51%)	Medium 54,458 Mean 54,469	Median 0 Mean 555
	HCW Sero positive	11/31 (35%)	Medium 51,713 Mean 51,078	Median 0 Mean 41		HCW Sero positive	16/31 (52%)	Medium 54,264 Mean 54,277	Median 85 Mean 795
	Patient- COVID-19 ARD	10/37 (27%)	Medium 51,168 Mean 51,268	Median 0 Mean 44		Patient- COVID-19 ARD	22/37 (59%)	Medium 54,278 Mean 54,411	Median 221 Mean 1091
Spike (median peak m/z -5,128)	HCW Sero negative	18/30 (60%)	Medium 51,117 Mean 51,078	Median 186 Mean 209	Spike (median peak m/z -54,284)	HCW Sero negative	25/30 (83%)	Medium 54,295 Mean 54,448	Median 889 Mean 1783
	HCW Sero positive	19/31 (61%)	Medium 51,140 Mean 51,212	Median 236 Mean 236		HCW Sero positive	21/31 (68%)	Medium 54,262 Mean 54,306	Median 433 Mean 1742
	Patient- COVID-19 ARD	34/37 (92%)	Medium 51,128 Mean 51,178	Median 507 Mean 554		Patient- COVID-19 ARD	31/37 (84%)	Medium 54,315 Mean 54,401	Median 623 Mean 2032

**Figure 4.** (A,B) Comparative table of IgG1 and IgG3 spectral analyses: Detection frequency, intensity and molecular mass for all samples captured by protein G , nucleocapsid  and prefusion .

complete spike protein [red box]. Further delineation is done by sample infection status: blue represents data from SARS-CoV-2 sero-negative HCWs, orange from SARS-CoV-2 sero-positive HCWs having recovered from mild symptoms and red sample data from convalescent patients recovering from COVID-19 ARDS.

Examining the average molecular mass of the IgG1 bound by or binding to the magnetic beads, although a wide variation of mass ( $\pm 800$   $m/z$ ) could be found between individual samples (Figure 2, Figure 4 A), no significant patterns could be detected as characteristics of any of the sample groups.

## 2.2. IgG3 Levels and Molecular Mass

Overall binding showed that protein G could bind IgG3 very rarely (peak detected in 24% of samples, median intensity 0AU) compared to that of the nucleocapsid (peak detected in 51% of samples, median intensity 103AU) and the prefusion spike protein (peak detected in 79% of samples, median intensity 630AU).

Although IgG3 is reported to be bound by protein G, this was low in our samples. Furthermore, Protein G almost completely failed to bind IgG3 in COVID-19 ARDS convalescent patient plasma (peak detected in 0 samples) and only in sero-negative (peak detected in 33% of samples) and sero-positive HCWs (peak detected in 39% of samples). Furthermore, the molecular mass of the IgG3 captured by protein G was uniform and consistent at 54,124–54,137  $m/z$  and never captured the larger IgG3 seen in the nucleocapsid and spike protein eluants (see Figures 4 and 5 and Figure 4B)

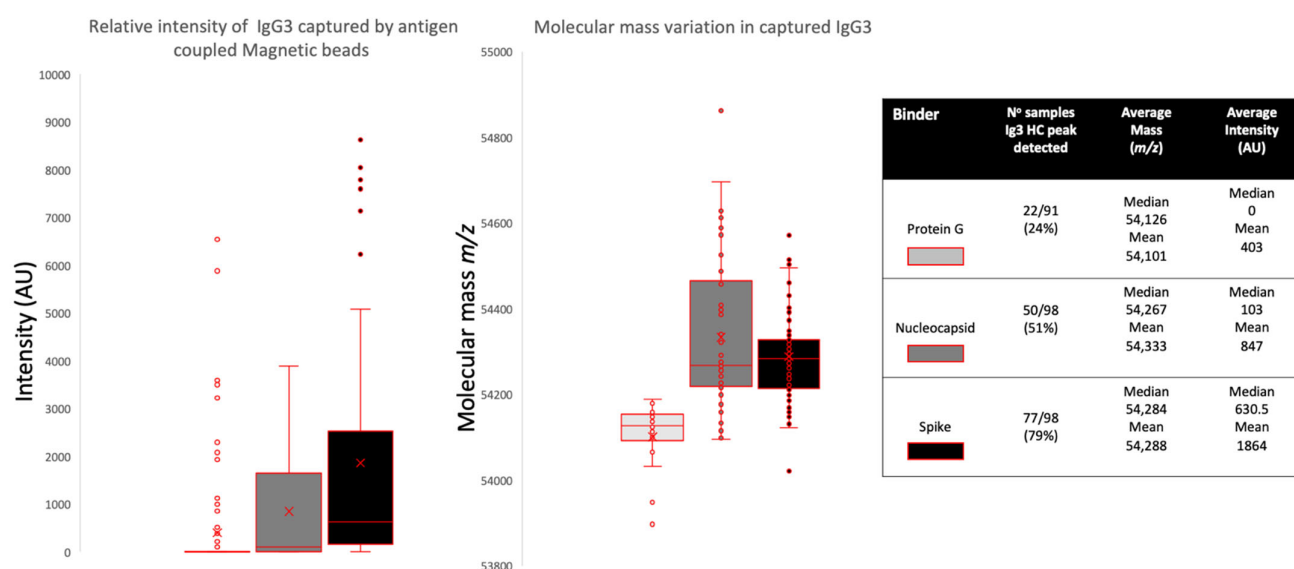


**Figure 5.** Relative intensities and variance in peak apex molecular mass of IgG3 heavy chains (IgG3 Hc) recovered from the same samples by protein G, nucleocapsid and stabilized spike protein. The non-parametric Kruskal–Wallis statistical test was carried out to test differences between study cohorts, the  $p$  values (alpha: 0.05) were as follows: intensity  $p < 0.0001$ , molecular mass  $p < 0.0001$ .



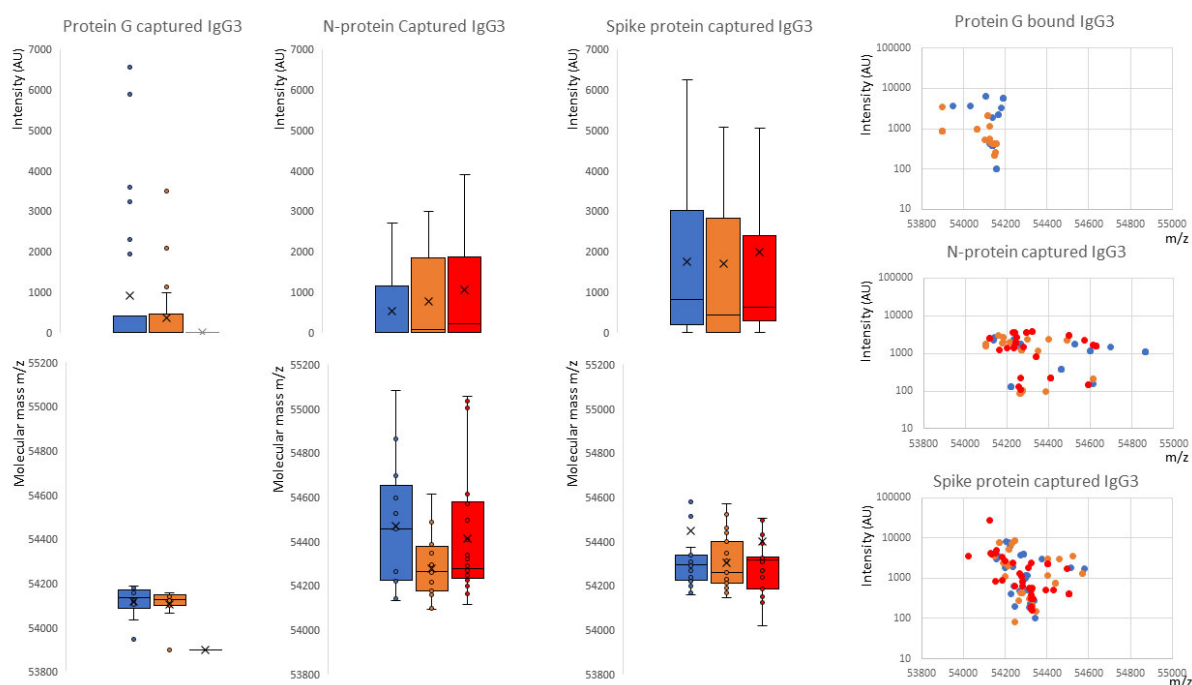


**Figure 6** Distribution of intensity for captured and eluted IgG3 heavy chains (IgG3 Hc) and the relative peak molecular masses bound and separated into sample groups. The dot plots to the right are intensity versus molecular mass for individual samples. Blue represents data from SARS-CoV-2 sero-negative HCWs, orange from SARS-CoV-2 sero-positive HCWs having recovered from mild symptoms and red sample data from convalescent patients recovering from COVID-19 ARDS. The non-parametric Kruskal–Wallis statistical test was carried out to test differences between study cohorts; the  $p$  values (alpha: 0.05) were as follows: protein G capture intensity  $p = 0.61$ , molecular weight  $p = 0.006$ ; protein N capture intensity  $p = 0.067$ , molecular weight  $p = 0.19$ ; protein S capture intensity  $p = 0.75$ , molecular weight  $p = 0.97$ .

The nucleocapsid showed an increased capture of IgG3 consistent with disease status: sero-negative HCWs (peak detected in 51% of samples, median intensity 0AU); sero-positive HCWs (peak detected in 52% of samples, median intensity 85AU); and convalescent plasma from COVID-19 ARDS (patients' peak detected in 59% of samples, median intensity 221AU). This reflects specific IgG3 sample antibodies binding the immobilized SARS-CoV-2 nucleocapsid and not a generic binding of total IgG3 by the nucleocapsid protein (see Figures 4B, 5 and 6). The median mass of the IgG3 heavy chains were 54,267  $m/z$ .

Spike proteins bound the most IgG3 and this was not consistent with disease status: sero-negative HCWs (peak detected in 83% of samples, median intensity 889AU); sero-positive HCWs (peak detected in 68% of samples, median intensity 443AU); and convalescent plasma from COVID-19 ARDS (patients' peak detected in 84% of samples, median intensity 623AU). This reflects the fact that immobilized SARS-CoV-2 prefusion spike proteins have a binding affinity for IgG3 antibodies, although anti-spike IgG3-specific binding cannot be excluded and would be masked in this system (see Figures 4B, 5 and 6). A distinctive feature of the IgG3 heavy chains detected in the spike protein capture experiments was the clear preference for a molecular species of around 54,284  $m/z$  (see Figures 4B, 5 and 6).

### 3. Discussion

The IgG subclasses have unique features associated with complement fixation and Fc receptor binding (see Table 1). The two most potent in this respect are IgG1 and IgG3, but IgG3 normally represents only 2–8% of the immunoglobulin found in serum and plasma, whilst IgG1 accounts for up to 70%. Here, IgG3 was evident as the more dominant IgG subtype in the humoral response to these SARS-CoV-2 antigens, along with another currently unidentified Ig with a heavy chain mass of ~49,000 *m/z* that could be IgG4.

The determination as to which Ig isotype is favored during the maturation of an immune response is influenced, in part, by cytokine stimulation of the germinal B cell during Ig heavy chain switching from IgM. Plasma cell formation is induced by interleukin (IL) - 21 but modulated by additional cytokines, such as IL-4 promoting switching to IgG and inhibiting switching to IgA. Conversely, IL-10 stimulates IgA production [13].

IgG3 has been reported as the dominant antibody in many viral infections [14]. Thus, it is perhaps unsurprising that IgG3 was the dominant captured subtype of IgG in this study. Interestingly, the nucleocapsid protein had a dominant IgG3 humoral patient response, whilst the spike protein also clearly induced a strong IgG1 humoral patient response.

However, unlike the pattern of the antibody binding to a solid-phase antigen seen in IgG1, the prefusion stabilized spike protein also appeared to have a non-specific binding affinity for IgG3, selectively binding IgG3 from the plasma of sero-negative HCWs, as well as that of patients and sero-positive HCWs. This was similar to our previously reported affinity of the prefusion spike protein for HSA, but of a higher mass form due to advanced glycation end product (AGE) modification (i.e., glycated albumin) [15].

The non-specific IgG3 capture by spike proteins also appeared to be of a higher mass than the low levels of IgG3 captured from the same samples by protein G (Figure 1). Indeed, protein G did not bind this higher molecular mass IgG3 found in the COVID-19 ARDS convalescent patient samples, despite these being the dominant IgG3 molecular mass form captured by the prefusion spike protein.

The mass differences represent only a 0.4% increase of these Ig Hc, but this would fit with the evasion–pathology hypothesis that SARS-CoV-2 binds serum proteins with specific glycan residues or reactive glycation end products [16]. Although immunoglobulins can be similarly AGE as a result of elevated reducing sugars in the blood [16], there is also the strong possibility that the specific variant/inherent glycosylation of IgG3 is the molecular target of this IgG3 binding–coating via prefusion spike protein. Changes in fucosylation and galactosylation of the IgG heavy chain Asparagine N (Asn)-linked glycans have been reported to be a feature of the humoral immune response of those developing ARDS as a result of COVID-19 [17–19]. However, there is little, if any, information concerning O-linked glycosylation variation and its effects on antibody bioactivity. IgG3 is unique amongst the IgG subtypes because it has three conserved O-linked glycosylation sites within each of its two defining heavy chain peptides that comprise the extended neck region (see Table 1) [20].

Previous studies in mice and humans suggest that different IgG subclasses show subclass-specific glycosylation patterns [21–24]. In particular, human IgG3 had less stem fucosylation and branch terminal galactose Asn-linked glycan moieties than IgG1 [24]. A bias towards IgG3 over IgG1 antibodies against the RBD of the spike protein has been reported to be associated with poor prognosis in COVID-19 ARDS patients [12]. Thus, the recent reports of reduced fucose and galactose saccharide residues in anti-SARS-CoV-2 IgG N-linked glycans isolated from patients with severe COVID-19 symptoms could be explained by a change in the ratio of IgG3 to IgG1 antibodies. However, the affinity for a specific higher mass form of IgG3 also points to a different post-translational modification, be it hyper glycosylation, glycation or a mixture of the two processes, which is associated with ARDS arising in individuals infected with SARS-CoV-2. This may prove to be not only a molecular marker of ARDS susceptibility in COVID-19 infected individuals, but



also directly related to molecular mechanisms by which SARS-CoV-2 can cause the various vascular and immunological pathologies described [25,26].

#### 4. Materials and Methods

##### 4.1. Samples

Serum and plasma samples were obtained from Health care workers (HCWs) and COVID-19 patients referred to the Royal Papworth Hospital for critical care during the first wave. NHS healthcare workers working at the Royal Papworth Hospital in Cambridge, UK served as the exposed HCWs cohort (Study approved by Research Ethics Committee Wales, IRAS: 96194 12/WA/0148. Amendment 5). NHS HCWs participants from the Royal Papworth Hospital were recruited through staff email over the course of two months (20 April 2020–10 June 2020) as part of a prospective study to establish sero-prevalence and immune correlates of protective immunity to SARS-CoV-2. Patients were recruited in convalescence either pre-discharge or at the first post-discharge clinical review. All participants provided written, informed consent prior to enrolment in the study. Sera from NHS HCWs and patients were collected between July and September 2020, approximately three months after they were enrolled in the study.

Representative convalescent serum and plasma samples from sero-negative HCWs, sero-positive HCWs and convalescent polymerase chain reaction (PCR)-positive COVID-19 patients were obtained for cross-sectional comparison. The serological screening to classify convalescent HCWs as either positive or negative was done according to the results provided by a CE-validated Luminex assay detecting N-, RBD- and S-specific IgG, a lateral flow diagnostic test (IgG/IgM) and an electrochemiluminescence immunoassay (ECLIA) detecting N- and S-specific IgG. Any sample that produced a positive result by any of these assays was classified as positive. Thus, the panel of convalescent plasma samples (three months post-infection) were grouped in three categories: (A) Sero-negative Staff ( $n = 30$  samples). (B) Sero-positive Staff ( $n = 31$  samples); and (C) Patients ( $n = 38$  samples) [27]. The age, sex and ethnicity of the three groups along with the co-morbidities found in the patient cohort are detailed in Supplementary Figure S1. As expected, there was an age bias toward older men in the patient cohort (see Supplementary Figure 1).

##### 4.2. Antigen-Coupled Magnetic Beads

Protein G-coupled magnetic beads were purchased from Cytivia Ltd. (Amersham Place, Little Chalfont, Buckinghamshire, UK). Recombinant nucleocapsid and recombinant stabilized complete spike protein magnetic beads were made by Bindingsite Ltd. (Birmingham, UK).

The viral spike protein (S protein) is present on virions as prefusion trimers with the receptor binding domain of the S1 region stochastically open or closed; an intermediary in the S1 region is cleaved and discarded and the S2 undergoes major conformational changes to expose and then retract its fusion peptide domain [28]. Here, the S protein was modified to disable the S1/S2 cleavage site and maintain the prefusion stochastic conformation [29].

##### 4.3. Semi-Automated Magnetic Bead Capture Processing

The processes of magnetic bead capture, washing, agitation and target binding protein elution can vary dramatically due to damage from overly vigorous mixing and yet, insufficient washing can result in the recovery of large amounts of non-specific binding proteins. To minimize these problems, as well as individual operator variability in the efficiency of target binding protein recoveries, the Crick automated magnetic rack system was employed. This has previously been described in full [15].

#### 4.4. Pre-Processing of the Magnetic Beads

1.5  $\mu\text{L}$  microcentrifuge tubes were loaded into the automated magnetic rack. Protein G (GE) and purified nucleocapsid or purified stabilized complete spike magnetic beads (Bindingsite, Birmingham, UK) in their buffer solutions were vortexed to ensure an even distribution of beads within the solution. 10  $\mu\text{L}$  of the appropriate magnetic beads were pipetted into each tube.

100  $\mu\text{L}$  of wash buffer, 0.1% Tween 20 in Dulbecco's phosphate-buffered saline (DPBS) was pipetted into each tube before resuspending. After mixing for several minutes, the instrument pulled the antigen beads to one side, allowing the wash buffer to be carefully discarded. The wash cycle was repeated three times.

#### 4.5. Sample Processing and Binding Fraction Elution from the Magnetic Beads

45  $\mu\text{L}$  of 10 x DPBS was pipetted into each of the tubes containing the washed magnetic beads. 5  $\mu\text{L}$  of vortexed neat plasma was pipetted and pump mixed into a tube containing the beads, repeating for each plasma sample. After the resuspension and automated mixing for 20 min, the beads were magnetically collected to one side and the non-bound sample was discarded. Three more wash cycles were conducted using 0.1% DPBS. Subsequently, another 3 wash cycles were conducted using ultra-pure water, discarding the water after the last cycle. 15  $\mu\text{L}$  of recovery solution (20 mM tris(2-carboxyethyl)phosphine (TCEP) (Sigma-Aldrich, Bournemouth, UK) + 5% acetic acid + ultra-pure water) was pipetted into the tubes. The tubes were run alternatively between the 'Resuspend' and 'Mix' setting for several minutes. After pulling the extracted magnetic beads to one side, the recovery solution was carefully removed using a pipette and placed into a clean, labelled 0.6  $\mu\text{L}$  microcentrifuge tube. This recovery solution was the eluant from the beads and contained the desired proteins.

#### 4.6. Sample Analysis by MALDI-ToF Mass Spectrometry

Mass spectra were generated using a 15 mg/mL concentration of sinapinic acid (SA) matrix. The elute from the beads was used to plate with no further processing. 1  $\mu\text{L}$  of the eluted samples were taken and plated on a 96-well stainless-steel target plate using a sandwich technique. The MALDI-ToF mass spectrometer (microflex<sup>®</sup> LT/SH, Bruker, Coventry, UK) was calibrated using a 2-point calibration of 2 mg/mL bovine serum albumin (33,200  $m/z$  and 66,400  $m/z$ ) (Pierce<sup>™</sup>, ThermoFisher Scientific, Waltham, MA, USA). Mass spectral data were generated in a positive linear mode. The laser power was set at 65% and the spectra were generated at a mass range between 10,000 to 200,000  $m/z$ ; pulsed extraction was set to 1400 ns.

A square raster pattern consisting of 15 shots and 500 positions per sample was used to give 7500 total profiles per sample. An average of these profiles was generated for each sample, giving a reliable and accurate representation of the sample across the well. The raw, averaged spectral data was then exported to a text file format to undergo further mathematical analysis.

#### 4.7. Spectral Data Processing

Mass spectral data generated by the MALDI-ToF instrument was uploaded to an open source mass spectrometry analysis software mMass<sup>™</sup> [30], where it was processed using a single-cycle, Gaussian smoothing method with a window size of 300  $m/z$ , and a baseline correction with applicable precision and relative offset depending on the baseline of each individual spectra. In software, automated peak picking was applied to produce peak lists, which were then tabulated and used in subsequent statistical analyses.

#### 4.8. Statistical Analysis

Peak mass and peak intensities were tabulated in Excel and plotted as graphic comparisons of distributions for each antigen capture and patient sample group. Means and

medians were calculated and, given the asymmetric distributions found, non-parametric statistics were applied, such as the Mann–Whitney U test, when comparing differences in group distributions.

## 5. Conclusions

The prefusion spike protein of SARS-CoV-2 has a binding affinity for serum IgG3, along with has, which is mediated via glycation and/or variance in inherent glycosylation. This may be part of an immune evasion/misdirection mechanism. The precise nature of the glycation–glycosylation profile in the susceptibility to, and pathogenesis of, COVID-19-related ARDS requires further study. In addition, humoral immune response reactivity indicates that a nucleocapsid induces a more dominant IgG3 response, whilst a spike protein induces both an IgG1 and IgG3 response. The ratio of IgG1 to IgG3 has been reported by Yates et al., [12] to be important in the development of ARDS and this also requires further investigation.

**Author Contributions:** Conceptualization, R.K.I., J.K.I. and J.H.; methodology, J.K.I., R.Z., D.R., C.S., G.W., R.P. and R.K.I.; formal data analysis, J.K.I., R.Z. and R.K.I.; investigation, J.K.I., R.Z., A.G., J.L. and R.K.I.; resources, R.K.I., J.H., S.H., J.L., D.R., C.S. and H.B.; data curation, J.K.I., R.Z., R.K.I., A.G. and J.L.; writing—original draft preparation, J.K.I. and R.K.I.; writing—review and editing R.Z., C.S., A.G., J.L., S.H., G.W., R.P., D.R., J.H. and H.B.; visualization, R.Z., A.G. and R.K.I.; supervision, R.K.I., S.H., J.H. and H.B.; project administration, J.K.I., H.B., S.H. and R.K.I.; funding acquisition, J.H., R.Z., S.H. and R.K.I. All authors have read and agreed to the published version of the manuscript.

**Funding:** This study was undertaken by the Humoral Immune Correlates to COVID-19 (HICC) consortium, funded by the UKRI and NIHR; grant number G107217 (COV0170-HICC: Humoral Immune Correlates for COVID-19). R.K.I. is also funded by NISAD Ideell Förening (charitable association) Organisations number 802528-6157.

**Institutional Review Board Statement:** This study was approved by the NHS Research Ethics Committee, Wales, IRAS: 96194 12/WA/0148. Amendment 5.

**Informed Consent Statement:** NHS HCWs participants from the Royal Papworth Hospital were recruited through staff email as part of a prospective study to establish sero-prevalence and immune correlates of protective immunity to SARS-CoV-2. Patients were recruited in convalescence, either pre-discharge or at the first post-discharge clinical review. All participants provided written, informed consent prior to enrolment in the study.

**Data Availability Statement:** Compiled summary data can be made available upon request to the corresponding author. Raw mass spectral data from the individual samples will require compiling from archives at MAPSciences and thus, a detailed project proposal justifying the additional resource expenditure necessary to provide this complete data set is required.

**Acknowledgments:** We gratefully acknowledge the loan of a prototype magnetic bead processing rack developed at the Francis Crick Institute London, UK, Bruker UK Ltd., (Coventry, UK) for the loan of the Microflex MALDI-ToF mass spectrometer. We also thank Erika Tranfield and Julie Green for their technical support with running and exporting the data from the Bruker Microflex.

**Conflicts of Interest:** The authors declare no conflicts of interest. The funders had no role in the design of the study, in the collection, analyses or interpretation of data, in the writing of the manuscript or in the decision to publish the results.

## Abbreviations

AGE	Advanced glycation end products
ARDS	Acute respiratory distress syndrome
Asn	Asparagine N
AU	Arbitrary units
DPBS	Dulbecco's phosphate-buffered saline
ECLIA	Electrochemiluminescence immunoassay

Fc	Fragment crystallizable
Hc	Heavy chain
HCWs	Health care workers
HSA	Human serum albumin
Ig	Immunoglobulin
MALDI-ToF	Matrix-assisted laser desorption ionization–time of flight
PCR	Polymerase chain reaction
RBD	Receptor binding domain
RSV	Respiratory syncytial virus
SA	Sinapinic acid
SDS-PAGE	Sodium dodecyl sulphate-polyacrylamide gel electrophoresis
TCEP	Tris(2-carboxyethyl)phosphine

## References

- Welker, C.; Huang, J.; Gil, I.J.N.; Ramakrishna, H. 2021 Acute respiratory distress syndrome update, with coronavirus disease 2019 focus. *J. Cardiothorac. Vasc. Anesth.* **2022**, *36*, 1188–1195. <https://doi.org/10.1053/j.jvca.2021.02.053>.
- Khadke, S.; Ahmed, N.; Ahmed, N.; Ratts, R.; Raju, S.; Gallogly, M.; De Lima, M.; Sohail, M.R. Harnessing the immune system to overcome cytokine storm and reduce viral load in COVID-19: A review of the phases of illness and therapeutic agents. *Virol. J.* **2020**, *17*, 154. <https://doi.org/10.1186/s12985-020-01415-w>.
- Cao, X. COVID-19: Immunopathology and its implications for therapy. *Nat. Rev. Immunol.* **2020**, *20*, 269–270. <https://doi.org/10.1038/s41577-020-0308-3>.
- Wang, W.; Xu, Y.; Gao, R.; Lu, R.; Han, K.; Wu, G.; Tan, W. Detection of SARS-CoV-2 in different types of clinical specimens. *JAMA* **2020**, *323*, 1843–1844. <https://doi.org/10.1001/jama.2020.3786>.
- Azkur, A.K.; Akdis, M.; Azkur, D.; Sokolowska, M.; Van De Veen, W.; Brügggen, M.-C.; O'Mahony, L.; Gao, Y.; Nadeau, K.; Akdis, C.A. Immune response to SARS-CoV-2 and mechanisms of immunopathological changes in COVID-19. *Allergy* **2020**, *75*, 1564–1581. <https://doi.org/10.5167/uzh-195056>.
- Post, N.; Eddy, D.; Huntley, C.; van Schalkwyk, M.C.; Shrotri, M.; Leeman, D.; Rigby, S.; Williams, S.V.; Bermingham, W.H.; Kellam, P.; et al. Antibody response to SARS-CoV-2 infection in humans: A systematic review. *PLoS ONE* **2020**, *15*, e0244126.
- Galipeau, Y.; Greig, M.; Liu, G.; Driedger, M.; Langlois, M.A. Humoral responses and serological assays in SARS-CoV-2 infections. *Front. Immunol.* **2020**, *11*, 3382.
- Voss, C.; Esmail, S.; Liu, X.; Knauer, M.J.; Ackloo, S.; Kaneko, T.; Lowes, L.E.; Stogios, P.J.; Seitova, A.; Hutchinson, A.; et al. Epitope-specific antibody responses differentiate COVID-19 outcomes and variants of concern. *JCI Insight* **2021**, *6*, e148855. <https://doi.org/10.1172/jci.insight.148855>.
- Robbiani, D.F.; Gaebler, C.; Muecksch, F.; Lorenzi, J.C.C.; Wang, Z.; Cho, A.; Agudelo, M.; Barnes, C.O.; Gazumyan, A.; Finkin, S.; et al. Convergent antibody responses to SARS-CoV-2 in convalescent individuals. *Nature* **2020**, *584*, 437–442. <https://doi.org/10.1038/s41586-020-2456-9>.
- Suthar, M.S.; Zimmerman, M.; Kauffman, R.; Mantus, G.; Linderman, S.; Vanderheiden, A.; Nyhoff, L.; Davis, C.; Adekunle, S.; Affer, M.; et al. Rapid generation of neutralizing antibody responses in COVID-19 patients. *Cell Rep. Med.* **2020**, *1*, 100040. <https://doi.org/10.1101/2020.05.03.20084442>.
- Atyeo, C.; Fischinger, S.; Zohar, T.; Slein, M.D.; Burke, J.; Loos, C.; McCulloch, D.J.; Newman, K.L.; Wolf, C.; Yu, J.; et al. Distinct early serological signatures track with SARS-CoV-2 survival. *Immunity* **2020**, *53*, 524–532.e4. <https://doi.org/10.1016/j.immuni.2020.07.020>.
- Yates, J.L.; Ehrbar, D.J.; Hunt, D.T.; Girardin, R.C.; Dupuis, A.P., II; Payne, A.F.; Sowizral, M.; Varney, S.; Kulas, K.E.; Demarest, V.L.; Howard, K.M. Serological analysis reveals an imbalanced IgG subclass composition associated with COVID-19 disease severity. *Cell Rep. Med.* **2021**, *2*, 100329.
- Lucas, C.L.; Kuehn, H.S.; Zhao, F.; Niemela, J.E.; Deenick, E.K.; Palendira, U.; Avery, D.T.; Moens, L.; Cannons, J.L.; Biancalana, M.; et al. Dominant-activating germline mutations in the gene encoding the PI(3)K catalytic subunit p110δ result in T cell senescence and human immunodeficiency. *Nat. Immunol.* **2014**, *15*, 88–97. <https://doi.org/10.1038/ni.2771>.
- Walker, M.R.; Eltahla, A.A.; Mina, M.M.; Li, H.; Lloyd, A.R.; Bull, R.A. Envelope-specific IgG3 and IgG1 responses are associated with clearance of acute hepatitis C virus infection. *Viruses* **2020**, *12*, 75. <https://doi.org/10.3390/v12010075>.
- Iles, J.; Zmuidinaite, R.; Sadee, C.; Gardiner, A.; Lacey, J.; Harding, S.; Ule, J.; Roblett, D.; Heeney, J.; Baxendale, H.; et al. SARS-CoV-2 spike protein binding of glycated serum albumin—Its potential role in the pathogenesis of the COVID-19 clinical syndromes and bias towards individuals with pre-diabetes/type 2 diabetes and metabolic diseases. *Int. J. Mol. Sci.* **2022**, *23*, 4126.
- Pampati, P.K.; Suravajjala, S.; Dain, J.A. Monitoring nonenzymatic glycation of human immunoglobulin G by methylglyoxal and glyoxal: A spectroscopic study. *Anal. Biochem.* **2011**, *408*, 59–63. <https://doi.org/10.1016/j.ab.2010.08.038>.
- Hoepel, W.; Chen, H.J.; Allahverdiyeva, S.; Manz, X.; Aman, J.; Bonta, P.; Brouwer, P.; de Taeye, S.; Caniels, T.; van der Straten, K.; et al. Anti-SARS-CoV-2 IgG from severely ill COVID-19 patients promotes macrophage hyper-inflammatory responses. *BioRxiv* **2020**. doi: <https://doi.org/10.1101/2020.07.13.190140>

18. Larsen, M.D.; de Graaf, E.L.; Sonneveld, M.E.; Plomp, H.R.; Nouta, J.; Hoepel, W.; Chen, H.J.; Linty, F.; Visser, R.; Brinkhaus, M.; et al. Afucosylated IgG characterizes enveloped viral responses and correlates with COVID-19 severity. *Science* **2021**, *371*, eabc8378.
19. Chakraborty, S.; Gonzalez, J.; Edwards, K.; Mallajosyula, V.; Buzzanco, A.S.; Sherwood, R.; Buffone, C.; Kathale, N.; Providenza, S.; Xie, M.M.; et al. Proinflammatory IgG Fc structures in patients with severe COVID-19. *Nat. Immunol.* **2021**, *22*, 67–73. <https://doi.org/10.1038/s41590-020-00828-7>.
20. Plomp, R.; Dekkers, G.; Rombouts, Y.; Visser, R.; Koeleman, C.A.; Lageveen-Kammeijer, G.; Jansen, B.C.; Rispen, T.; Hensbergen, P.; Vidarsson, G.; et al. Hinge-region O-glycosylation of human immunoglobulin G3 (IgG3). *Mol. Cell. Proteom.* **2015**, *14*, 1373–1384. <https://doi.org/10.1074/mcp.m114.047381>.
21. Kao, D.; Lux, A.; Schaffert, A.; Lang, R.; Altmann, F.; Nimmerjahn, F. IgG subclass and vaccination stimulus determine changes in antigen specific antibody glycosylation in mice. *Eur. J. Immunol.* **2017**, *47*, 2070–2079. <https://doi.org/10.1002/eji.201747208>.
22. De Haan, N.; Reiding, K.R.; Krištić, J.; Ederveen, A.H.; Lauc, G.; Wuhler, M. The N-glycosylation of mouse immunoglobulin G (IgG)-fragment crystallizable differs between IgG subclasses and strains. *Front. Immunol.* **2017**, *8*, 608–608. <https://doi.org/10.3389/fimmu.2017.00608>.
23. Zaytseva, O.O.; Jansen, B.C.; Hanić, M.; Mrèla, M.; Razdorov, G.; Stojković, R.; Erhardt, J.; Brizić, I.; Jonjić, S.; Pezer, M.; et al. MlgGGly (mouse IgG glycosylation analysis)—A high-throughput method for studying Fc-linked IgG N-glycosylation in mice with nanoU-PLC-ESI-MS. *Sci. Rep.* **2018**, *8*, 13688. <https://doi.org/10.1038/s41598-018-31844-31841>.
24. Wiczorek, M.; Braicu, E.I.; Oliveira-Ferrer, L.; Sehouli, J.; Blanchard, V. Immunoglobulin G subclass-specific glycosylation changes in primary epithelial ovarian cancer. *Front. Immunol.* **2020**, *11*, 654. <https://doi.org/10.3389/fimmu.2020.00654>.
25. Costa, L.B.; Perez, L.G.; Palmeira, V.A.; Macedo e Cordeiro, T.; Ribeiro, V.T.; Lanza, K.; Silva, A.C.S.E. Insights on SARS-CoV-2 molecular interactions with the renin-angiotensin system. *Front. Cell Dev. Biol.* **2020**, *8*, 559841. <https://doi.org/10.3389/fcell.2020.559841>.
26. Sood, S.; Aggarwal, V.; Aggarwal, D.; Upadhyay, S.K.; Sak, K.; Tuli, H.S.; Kumar, M.; Kumar, J.; Talwar, S. COVID-19 Pandemic: From molecular biology, pathogenesis, detection, and treatment to global societal impact. *Curr. Pharmacol. Rep.* **2020**, *6*, 212–227. <https://doi.org/10.1007/s40495-020-00229-2>.
27. Castillo-Olivares, J.; Wells, D.A.; Ferrari, M.; Chan, A.; Smith, P.; Nadesalingam, A.; Paloniemi, M.; Carnell, G.; Ohlendorf, L.; Antoni, D.; et al. Towards internationally standardised humoral immune correlates of protection from SARS-CoV-2 infection and COVID-19 disease. *medRxiv* **2021**. doi: <https://doi.org/10.1101/2021.05.21.21257572>
28. Song, W.; Gui, M.; Wang, X.; Xiang, Y. Cryo-EM structure of the SARS coronavirus spike glycoprotein in complex with its host cell receptor ACE2. *PLoS Pathog.* **2018**, *14*, e1007236. <https://doi.org/10.1371/journal.ppat.1007236>.
29. Carnell, G.W.; Ciazynska, K.A.; Wells, D.A.; Xiong, X.; Aguinam, E.T.; McLaughlin, S.H.; Mallery, D.; Ebrahimi, S.; Ceron-Gutierrez, L.; Asbach, B.; et al. SARS-CoV-2 spike protein stabilized in the closed state induces potent neutralizing responses. *J. Virol.* **2021**, *95*, e00203–21.
30. Strohm, M.; Kavan, D.; Novák, P.; Volný, M.; Havlíček, V. *mMass 3*: A cross-platform software environment for precise analysis of mass spectrometric data. *Anal. Chem.* **2010**, *82*, 4648–4651. <https://doi.org/10.1021/ac100818g>.